Energy and AI 25 (2026) 100790

Contents lists available at ScienceDirect

Energy and AI

journal homepage: www.elsevier.com/locate/egyai

Data-driven degradation analysis of proton exchange membrane electrolyzer stacks under dynamic load operation

H. Sayed-Ahmed [a], R. Keller [b], Á.I. Toldy [a], M. Müller [b], D. Froning [b], A. Santasalo-Aarnio [a,*]

[a] Department of Energy and Mechanical Engineering, Aalto University, FI-00076 Espoo, Finland
[b] Forschungszentrum Jülich GmbH, Institute of Energy Technologies, IET-4: Electrochemical Process Engineering, Jülich, D-52425, Germany

HIGHLIGHTS

- Degradation of PEM stacks affects the profitability of electrolysis dynamic operation.
- Partial loading decreases the degradation rate of PEM electrolyzer stacks.
- Minimizing rate of change of current density limits the increase in degradation rate.

GRAPHICAL ABSTRACT

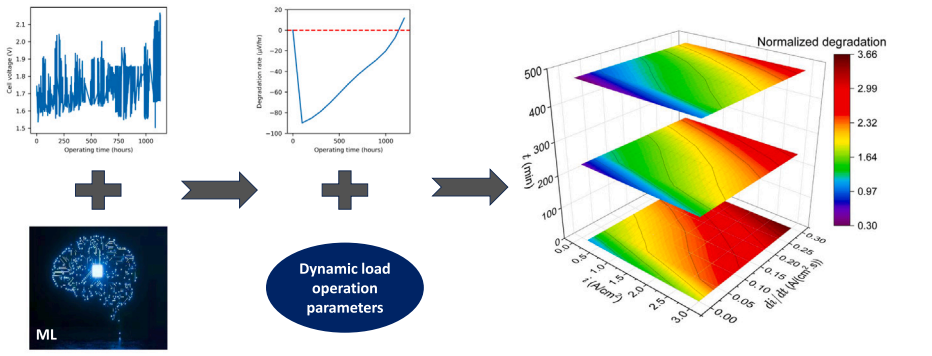

ARTICLE INFO

Dataset link: https://doi.org/10.26165/JUELICH-DATA/FEKKSS

Keywords:
PEM electrolysis
Dynamic operation
Degradation rate
Machine learning

ABSTRACT

Dynamic load operation of proton exchange membrane (PEM) electrolyzers offers a significant opportunity to reduce the cost of green hydrogen, by quickly adjusting their hydrogen production rates in response to low electricity prices. However, this operation mode affects the degradation rate of PEM electrolyzer stacks differently compared to steady-state operation. This study aims to analyze the effects of dynamic load operation parameters on the degradation rate of PEM electrolyzer stacks and to provide suggestions to mitigate some of their negative implications. A feed-forward deep neural network model was developed using experimental data from two 50 kW PEM stacks (each operated for 1134 h). This model was able to evaluate the PEM stack degradation at different operating conditions. It was observed that partial load operation decreased the degradation rate of PEM electrolyzer stacks by up to 69%. Moreover, the degradation rate at 0.3 A/(cm^2·s) rate of change in current density and low load cycling time was 266% higher than the degradation rate during steady-state operation. Although dynamic load operation increases the degradation rate compared to steady-state operation, optimizing the operation parameters can limit this increase in the degradation rate.

1. Introduction

Decreasing the levelized cost of hydrogen (LCOH) is a necessity to decarbonize the energy sector and improve the profitability of green hydrogen projects [1–3]. In addition to reducing the capital costs of electrolysis plants, it is necessary to minimize the operational costs [4–6]. Assuming specific installation costs of 500 €/kW, electricity costs of 0.04 €/kWh, and 60,000 full load hours, the electricity cost contributes to more than 80% of the LCOH [7,8]. Therefore, optimizing the operation of electrolysis plants and maximizing production at low electricity prices have the potential to reduce LCOH [9–11].

* Corresponding author.
E-mail address: annukka.santasalo@aalto.fi (A. Santasalo-Aarnio).

https://doi.org/10.1016/j.egyai.2026.100790
Received 25 March 2026; Received in revised form 15 May 2026; Accepted 26 May 2026
Available online 1 June 2026

Abbreviations

DNN	deep neural network
LCOH	levelized cost of hydrogen
PEM	proton exchange membrane
RCCD	rate of change in current density

In previous work, it was observed that the dynamic load operation of proton exchange membrane (PEM) electrolysis reduces the LCOH by up to 42% compared to the steady-state operation [12]. However, each 1 μV/h increase in the average cell voltage degradation rate of the electrolyzer stack over its lifetime increases the LCOH by up to 2.2% [12]. Cell voltage degradation rate is used to quantify the average decline in electrolyzer stack performance over time [13,14]. As the degradation rate increases, the consumed electricity to produce a comparable amount of green hydrogen also increases [15–17].

This dependency between the degradation rate and the LCOH shows the significance of understanding and predicting the degradation rate for reducing green hydrogen cost. Values for degradation rates from 2.5 to 50 μV/h were identified in Rakousky et al. [18], Papakonstantinou et al. [19], and Panto et al. [20]. Generally, degradation rates are affected by both operational parameters and strategies.

Wallnöfer-Ogris et al. [14] studied the degradation mechanisms and the most influential factors that affect the lifetime of PEM electrolyzer stacks. They classified the influence of the operating parameters on the degradation mechanisms as high, significant, and possible. They observed that high current densities, transient operation, start–stop cycling, temperature higher than 80 °C, high hydrogen pressure, and impurities in water and balance-of-plant have high influence on different degradation mechanisms.

The dynamic load operation of electrolyzers can be characterized by three key operating parameters: current density levels, load cycling time, and rate of change in current density (RCCD). High and very low operating current densities decrease the lifetime of PEM electrolyzer stacks [21]. Rakousky et al. [18] measured the degradation rate for steady-state operation at current densities of 1 A/cm^2 and 2 A/cm^2. They demonstrated that increasing the current density increases the degradation rate (from 0 to 194.25 μV/h). Besides, Gago et al. [22] examined the effect of peak current density on the degradation rate of PEM electrolyzer stacks. They experimented with peak current densities of 2 A/cm^2, 3 A/cm^2, 4 A/cm^2, and 4.5 A/cm^2. They identified that higher peak current density escalated the irreversible degradation of the electrolyzer stack.

Frensch et al. [23] simulated fluoride emission rates in terms of current density and temperature. High fluoride emission rates indicate an increase in the thinning of membrane and ionomer in the catalyst layer [24]. Frensch et al. illustrated that decreasing the current density of PEM electrolyzers from 2 A/cm^2 to 0.2 A/cm^2 at 80 °C, increased the fluoride emission rates from 0.64 μg/(cm^2·h) to 3.3 μg/(cm^2·h). Moreover, Chandesris et al. [25] observed that the fluoride emission rate was maximum at current densities of 0.2 A/cm^2 and 0.4 A/cm^2 at operating temperatures of 60 °C and 80 °C respectively.

Load cycling time is defined as the duration for which the current density is maintained at a constant level before transitioning to a different current density level. Alia et al. [26] studied the degradation of PEM electrolyzer stacks at different load cycling times. The load cycling times were 5, 15, 30, and 60 s, where cell voltage cycled between 1.45 V and 2 V. Alia et al. observed that decreasing the load cycling time increases the degradation of the electrolyzer stack. Similar findings have been presented by Rakousky et al. [18] that examined the degradation rate at load cycling times of 10 min and 6 h. They showed that decreasing the load cycling time, from 6 h to 10 min, increased the degradation rate from 15.86 μV/h to 49.55 μV/h correspondingly.

In Su et al. [27] and Voronova et al. [28], not only does the current density increase the degradation rate, but also square-wave modes with different rates of changes in currents and high dynamic photovoltaic profiles have been shown to influence the degradation rate. In general, a high RCCD increases the degradation rate [29]. He et al. [30] examined the effect of the RCCD on the degradation rate of PEM electrolyzer stacks using two flow field configurations. They found that the degradation rate at step load cycling was 2.45 and 1.61 times the multi-step load cycling using parallel flow field and triple serpentine flow field respectively.

Conversely, Xu et al. [31] developed a deep learning model to predict and compare the degradation of a PEM electrolyzer stack in constant and start–stop cycling mode. They found that the degradation rate under start–stop cycling was lower than the degradation rate at constant operation. However, the current density in the constant mode was 3 A/cm^2, while the current density fluctuated between 1.5 A/cm^2 and zero at the start–stop mode. This difference in the current density can be the cause of the lower degradation rate. Therefore, a comprehensive understanding of the interrelation between current density levels, the RCCD, and load cycling time is essential to optimize system performance and mitigate degradation phenomena.

These limitations highlight a gap in the existing literature: it is not sufficient to study the effect of individual parameters or their limited combinations to optimize system performance and mitigate degradation. In fact, this can only be achieved through a comprehensive understanding of the interrelation between current density levels, the RCCD, and load cycling time. This study bridges this gap by investigating the performance of a 100 kW electrolyzer, operating two 50 kW PEM stacks in parallel, each with more than 1000 operating hours. The study focuses on the effect of dynamic load operation parameters (current density levels, RCCD, and load cycling time) and their interactions on the degradation rate of PEM electrolyzer stacks.

2. Methodology

This section describes the experimental setup and the model used to calculate the average cell voltage degradation rate at different operating conditions.

2.1. Experimental setup

Fig. 1 depicts a 100 kW PEM electrolyzer system installed at IET-4 (Institute of Energy Technologies - Electrochemical Process Engineering) of Forschungszentrum Jülich, comprising key components essential for operational functionality. Central to the PEM system are the electrolysis cells, in which water is electrochemically split into hydrogen and oxygen under the influence of applied electric power. The system design is based on two 50 kW PEM stacks, operated in parallel, visible in the lower left quadrant of Fig. 1. This configuration was selected to accommodate the high power input requirements while mitigating design challenges associated with scaling. Specifically, the number of cells per stack was limited to 27 to reduce the potential risk of stack failure due to an uneven performance distribution associated with large series-connected cell assemblies. Furthermore, the active cell area was 300 cm^2. This is an order of magnitude in which the interactions between stack and system are realistically mapped, and at the same time, a high degree of flexibility in the choice of operating conditions is given. The complete specification of one 50 kW PEM stack can be found in Table 1. The test rig was engineered for a maximum operating pressure of 50 bar on both the cathode and the anode side. Table 2 summarizes the operating parameters.

Fig. 2 shows a simplified process flow diagram, indicating the key components for the operation of the system. Among these is the rectifier, which is essential for supplying a stable direct current (DC) to the electrochemical process. Since the electrical grid delivers an alternating current (AC), the rectifier converts it into DC to enable controlled and

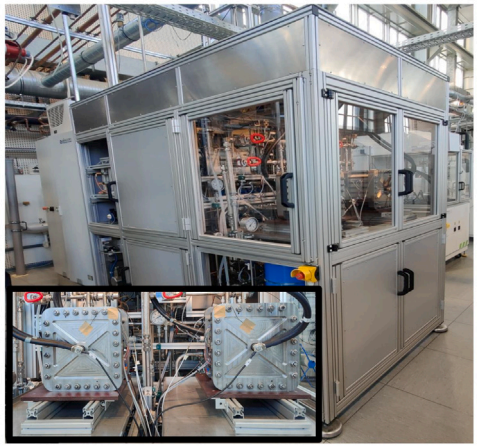

Fig. 1. Test rig 100 kW PEM electrolyzer with two 50 kW PEM stacks.

Table 1
Specification 50 kW PEM stack operating in 100 kW PEM electrolyzer.

Specification	Value	Unit	Stack image
Number cells	27		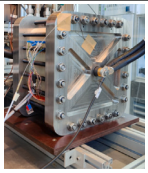
Maximal power	6	$\frac{W}{cm^2}$	
Coating cathode	Pt 0.940	$\frac{mg}{cm^2}$	
Coating anode	Ir 2.610	$\frac{mg}{cm^2}$	
Membrane	Nafion 117		
Cell area	300	cm^2	
Bipolar plates	metal		

Table 2
Operating parameters 100 kW PEM electrolyzer derived from the public available data set [32].

Specification		Value	Unit
Cell voltage	U_{cell}	0..2	V
Current density	j_{el}	0..3	$\frac{A}{cm^2}$
Pressure anode	p_{O_2}	0..50	bar
Pressure cathode	p_{H_2}	0..50	bar
Temperature	T_{Stack}	60..80	°C
Specific volume flow anode	$\dot{V}_{anode}$	0..10	$\frac{ml}{min\ cm^2}$
Specific volume flow cathode	$\dot{V}_{cathode}$	0..10	$\frac{ml}{min\ cm^2}$

continuous operation of the PEM electrolyzer. Furthermore, the two circulation pumps in the anode and cathode loops can be identified as essential components for operational functionality. These pumps ensure the continuous supply of reactants to the electrochemical reaction and realize the temperature control of the PEM stack. Each loop is equipped with a heating element and a plate heat exchanger for cooling. During cold start-up, the heating elements provide baseline preheating to enable the initial operation of the PEM stack. As the system reaches higher temperatures during operation, the plate heat exchangers are activated to dissipate excess heat. Throughout nominal operation, the temperature of the PEM stack T_{Stack} is maintained primarily by the cooling system. The nominal stack temperature range of the 100 kW system lies between 60 and 80 °C (Table 2). The circulation of water on both sides leads to a two-phase flow regime under load conditions, consisting of reaction gas and liquid water. This two-phase mixture is separated in gas separators, and the water vapor in the gas fraction is condensed before the product gases are discharged. With the drain valves on both sides, the pressure of hydrogen p_{H_2} and oxygen p_{O_2} can be controlled. Additionally, the flow diagram indicates a water dosing unit, which replenishes the water consumed during the electrochemical reaction.

2.2. Measurements performed 100 kW electrolyzer

All experimental measurements analyzed in this work were carried out by using the 100 kW PEM electrolyzer system in Fig. 1 [32]. Over the years, the 100 kW system was operated under an extensive range of scenarios, including renewable energy profiles, thermally dynamic sequences, and tailored ramping loads, resulting in numerous peer-reviewed publications. Among these, experiments with system dynamics and the impact of renewable energy sources on systems design have been performed within Rauls et al. [33], where the system was subjected to dynamic load profiles derived from photovoltaic and wind power data. In addition, the cold-start behavior of the system was evaluated, and the results, including various start-up scenarios and their implications, were published by Rauls et al. [34]. Further measurements were conducted to validate a feedforward model-based temperature control strategy by Keller et al. [35]. Operational strategies, such as dynamic ramping under variable load conditions, were also tested and validated using the 100 kW system for a variety of scenarios by Keller et al. [36]. Beyond the experiments associated with specific publications, additional long-term operational tests, commissioning procedures, and load profile applications were carried out to support the development and validation of an adaptive pressure control strategy.

The operational history of the 100 kW PEM electrolyzer spans a period of six years, during which the system was exposed to a diverse set of operational modes. This includes periods of continuous operation as well as extended shutdowns. The resulting database serves as the basis for an aging analysis using artificial intelligence methodologies. The data exhibit a high degree of temporal and operational variability: on one hand, highly dynamic measurements with 1 Hz resolution were performed under PV and wind-based load conditions; on the other hand, phases with step changes in current density and steady-state operation were also included. In addition to electrical input, temperature plays a critical role in system aging. Particularly during start-up phases, temperature control development, and dynamic ramping experiments, the system experienced high thermal gradients and fluctuations.

2.3. Modeling

Experimental data, 945068 data points measured during 1134 h of operation, was used to develop a deep neural network (DNN) model to predict the cell voltage in terms of operating time. Afterwards, the model was used to calculate the PEM stack voltage degradation rate with a focus on dynamic load operation parameters. The average degradation rate was calculated as shown in Eq. (1) [37]. The average cell voltages were predicted at identical operating conditions.

$$\text{Degradation Rate} = \frac{\sum_{i=1}^{N}(V(t_i + \Delta t_i) - V(t_i))}{\sum_{i=1}^{N} \Delta t_i} \quad (1)$$

$V(t_i)$ is the cell voltage at any specific time, $V(t_i + \Delta t_i)$ is the subsequent cell voltage, and Δt_i is the time difference between $V(t_i)$ and $V(t_i + \Delta t_i)$.

Fig. 4 shows the configuration of the feed-forward DNN used to predict the cell voltage in terms of operating time and the 13 input parameters used in the model. The model consisted of one normalization input layer, six hidden layers, and one output layer. Each hidden layer included 32 neurons. Fig. 4 shows the activation function of each hidden layer (mish, swish, or linear). Eq. (2) shows the mish activation function, while Eq. (3) shows the swish activation function [38,39].

$$mish(x) = x \cdot \tanh(\ln(e^x + 1)) \quad (2)$$

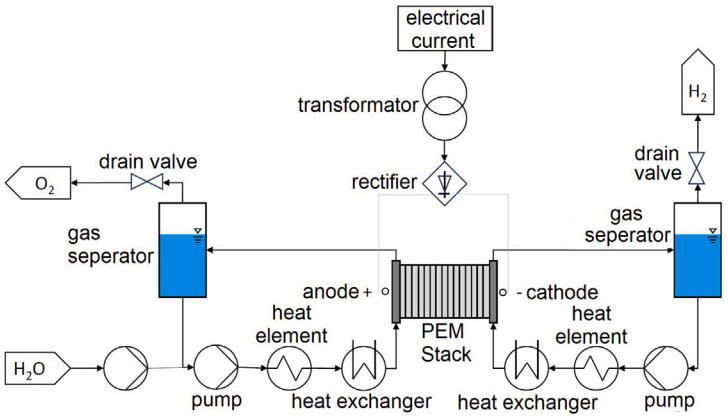

Fig. 2. Simplified process flow diagram of the 100 kW PEM electrolyzer.

$$swish(x) = x \cdot \frac{1}{1+e^{-x}} \tag{3}$$

Data from two 50 kW PEM electrolyzer stacks were used to train the model. Nevertheless, for improving the model accuracy, stack labels (0 and 1) were added to account for the differences of the voltage prediction in the two stacks. Moreover, current density was limited between 5% and 100% of the rated current density. Cycling between on and off states was not included in this model to avoid the excessive increase in the degradation rate of PEM stacks caused by frequent on/off cycles [40].

Fig. 3 shows the experimental cell voltage of the two stacks, used to train and evaluate the model, as a function of operating time derived from [32]. Fig. 3 reflects the highly dynamic operation of the PEM electrolyzer stacks over time. The observed fluctuations in cell voltage are primarily caused by variations in operating conditions, particularly changes in current density and stack temperature, to which the cell voltage responds directly. Due to these continuously changing operating conditions, the curve does not allow a direct assessment of degradation, since such an analysis would require constant operating parameters (e.g., fixed current density and temperature). However, it can be observed that after approximately 1000 h of operation, the overall trend of the cell voltage shifts towards higher values, which is indicative of degradation effects. At the same time, the cell voltage remains within the typical operating range of the system.

The experimental data of the two stacks were randomly divided into training, calibration, and testing datasets with a 8:1:1 ratio. The training dataset was used to train the feed-forward DNN. The calibration dataset was used to perform the uncertainty analysis of the model, using split conformal prediction and bootstrapping residuals methods [41,42]. The testing dataset was used to evaluate the model and the empirical coverage of the prediction intervals. During training the model, the training dataset was divided into training and validation datasets with a 4:1 ratio. The model stopped training (updating the weights) when the validation accuracy did not improve for three consecutive epochs. More details about the model can be found in Appendix.

3. Results and discussion

This section discusses the change in the degradation rate of PEM electrolyzer stacks as a result of dynamic load operation. The section focuses on the effect of current density levels, RCCD, and load cycling time on the degradation rate. These factors were chosen as they describe the difference in load operation between steady-state and dynamic load operation modes. This allows for a comparison between the degradation rate under dynamic load operation with the steady-state operation degradation rate given by the manufacturer.

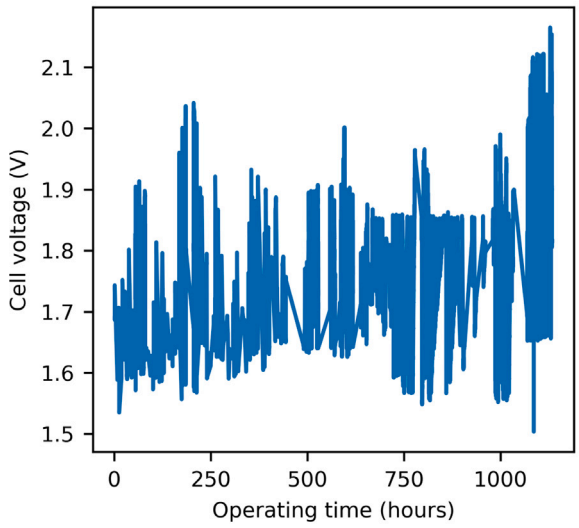

Fig. 3. Experimental cell voltage as a function of operating time.

3.1. Model validation

The DNN model was validated using the introduced experimental data of the 100 kW PEM electrolyzer. The coefficient of determination (R^2) and root mean square error ($RMSE$) of the training dataset were 0.9989 and 0.00322 V respectively, while R^2 and $RMSE$ of the testing dataset were 0.9988 and 0.00332 V respectively. Fig. 5 shows the distribution of the residuals. The residuals for predicting the cell voltage are centered around 0.00127 V with standard deviation of 0.00288 V and skewness of −1.089. The standard deviation of the experimental data was 0.097 V. These values indicate the accuracy of the model in predicting the average cell voltage under different operating conditions. Moreover, similar R^2 and $RMSE$ values in training and testing datasets, high ratio between training dataset and trainable parameters (105:1), and early stopping of the model training when the validation accuracy did not improve for three consecutive epochs suggest that the model is not overfitting.

Finally, Fig. 6 displays the predicted cell voltage residuals as a function of operating time. As illustrated, the model accurately predicts the cell voltage over time.

3.2. Degradation rate

Even though there was a significant amount of experimental data from the two PEM electrolyzer stacks, the operational parameters were

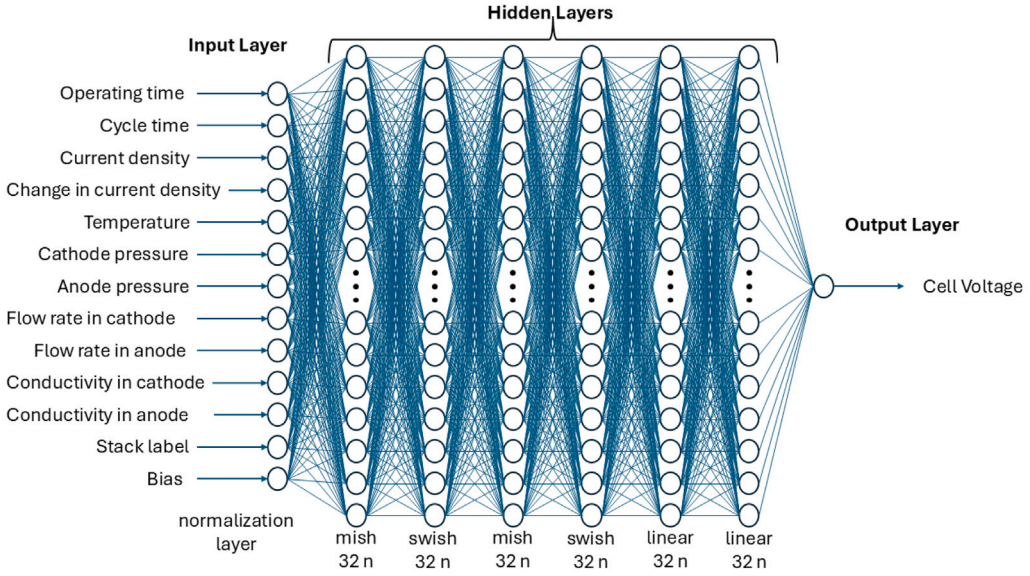

Fig. 4. Feed-forward deep neural network model.

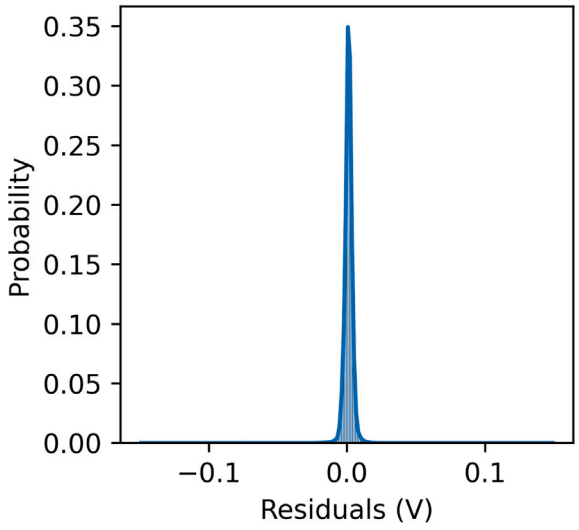

Fig. 5. Combined cell voltage residuals distribution of the two stacks.

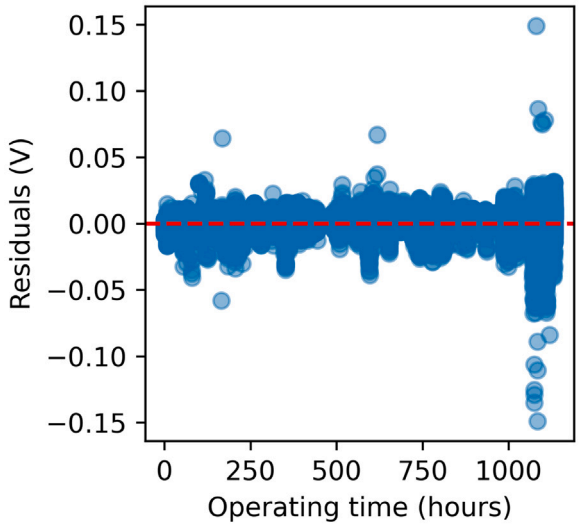

Fig. 6. Predicted cell voltage residuals over operating time of the two stacks.

highly variable, and the degradation rate had to be inferred indirectly. Therefore, DNN model was applied to investigate the change in the degradation rate of the two PEM electrolyzer stacks over their operating times, which is illustrated in Fig. 7.

As shown in Fig. 7, there was an initial improvement in the performance of the PEM stacks in the first 100 h of operation. However, by the end of the operation time, the average cumulative degradation rate of the two stacks was 11.7 μV/h.

3.3. Uncertainty analysis

The DNN model uncertainty was quantified using split conformal prediction and bootstrapping residuals methods. The split conformal prediction method computed the conformal quantile at 95% confidence level. The conformal quantile was 5.87 mV. This corresponds to a symmetric uncertainty prediction interval of ±5.87 mV at any prediction point (total prediction interval width equaled to 11.74 mV). The empirical coverage, calculated using the testing dataset, reached 95.02%. This corresponds to uncertainty in the degradation rate after 1134 h of operation equals to ±7.32 μV/h. The lower uncertainty value compared to the predicted degradation rate indicates that the model captures the degradation of the stacks.

The bootstrapping residuals method yielded an empirical coverage of 94.82% and a mean total prediction interval width of 10.86 mV, with a minimum and maximum intervals equal to 8.99 mV and 13.71 mV respectively. The close agreement between both methods confirms the robustness and consistency of the uncertainty estimates. Fig. 8 shows the total uncertainty prediction interval width computed using split conformal prediction and bootstrapping residuals methods.

3.4. Dynamic load operation parameters

Fig. 9 demonstrates the effect of varying the current density, RCCD, and load cycling time on the degradation rate of the two PEM electrolyzer stacks. The change in degradation rates was normalized by the degradation rate at steady-state operation and rated current density to generalize the findings of the study, since electrolyzer stacks from different manufacturers and different batches have different degradation rates.

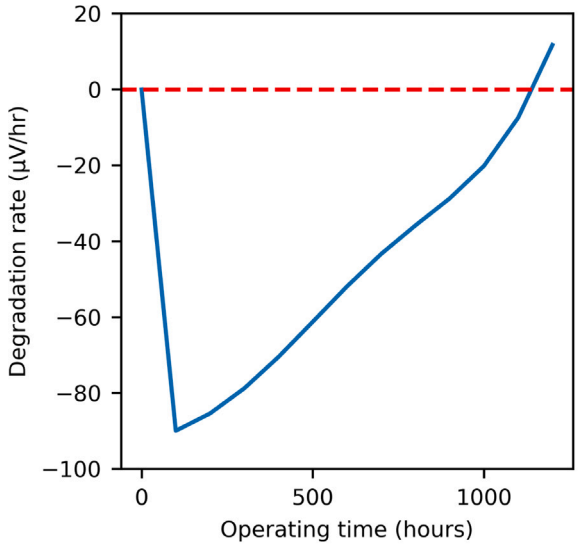

Fig. 7. Combined degradation rate of the two stacks.

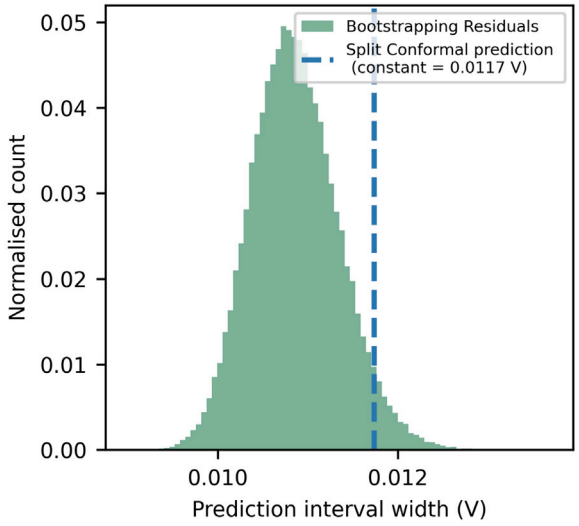

Fig. 8. Uncertainty prediction interval width.

As demonstrated in Fig. 9, partial load operation decreases the degradation rate. Within this model, at a current density corresponding to 5% of the rated value (0.15 A/cm^2), the degradation rate reduces by 69% relative to that observed at a current density of 3 A/cm^2. Additionally, decreasing the load cycling time increases the degradation rate. At one hour cycling time, the degradation rate increases by 64% compared to eight hours cycling time.

Moreover, Fig. 9 highlights that the degradation rate increases steeply with an increasing RCCD. The RCCD is affected by both the amplitude of the fluctuations and the step size. The degradation rate at 0.3 A/(cm^2·s) increases by 183% compared to steady-state operation (0 A/(cm^2·s)).

The direct correlation between the current density and the degradation rate aligns with the findings of Bahr et al. [43] and Su et al. [27]. Bahr et al. [43] calculated the degradation rates at 0.1 A/cm^2, 1.2 A/cm^2, and 2 A/cm^2. They observed that the degradation rate reduced from 22.1 μV/h at 2 A/cm^2 to 15.2 μV/h and 9.7 μV/h at 1.2 A/cm^2 and 0.1 A/cm^2 respectively. In other words, the ratio between the degradation rate at 1.2 A/cm^2 and the degradation rate at 2 A/cm^2 was about 69%. This value is close to the degradation rate ratio calculated by the DNN developed in this study at the same current densities (71%)

Similarly, Su et al. [27] measured the degradation of PEM electrolyzer stacks at different current densities. They found that the degradation rate increased from 22 μV/h at 1 A/cm^2 to 50 μV/h at 3 A/cm^2. The ratio between the degradation rate at 1 A/cm^2 and 3 A/cm^2 was 45%, that is well in line with the obtained results in this study (48%).

In terms of load cycling time, Rakousky et al. [18] found that decreasing cycling time from 6 h to 10 min increased the degradation rate by 212%. The current density was varied between 0 and 2 A/cm^2. In this work, decreasing the cycling time from 6 h to 10 minutes increases the degradation rate by 121%, assuming the RCCD is constant in both scenarios. However, if the RCCD is different in both scenarios (maximum 0.3 A/(cm^2·s) at 10 min cycling interval), the degradation rate increases by up to 450%.

Finally, Yung et al. [44] and He et al. [30] studied the influence of RCCD on the degradation rate of PEM electrolyzer stacks. Yung et al. [44] demonstrated that increasing the ramping rate from 30 mV/s to 300 mV/s increased the degradation rate from 0.36 to 1.26 mV/h, corresponding to an increase of about 250%. These ramping rates were equivalent to 0.36 A/(cm^2·s) and 3.94 A/(cm^2·s) respectively. He et al. [30] observed that RCCD of 0.4 A/(cm^2·s) increased the degradation rate by 80% to 220% compared to steady-state operation, depending on the flow field configuration. Although the values of RCCD used in these studies are outside the boundaries of the DNN model developed in this paper, the same trend persists. Increasing the RCCD increases the degradation rate of PEM electrolyzer stacks: at 0.3 A/(cm^2·s) the degradation rate increased by 183% compared to steady-state operation.

Fig. 10 demonstrates the combined effect of the dynamic load operation parameters on the degradation rate. As shown in Fig. 10, the degradation rate ranged from 0.3 to 3.66 times the degradation rate at steady-state operation and rated current density. The degradation rate was at its maximum at high current densities, high RCCDs, and short load cycling times.

In general, the strategy of operation should consider both the technical requirements of the system and how these requirements affect the lifetime of the electrolyzer stack. If a high RCCD is needed, for example, when participating in frequency containment reserve for disturbances electricity reserve market [45], it is advisable to prioritize operating at high load cycling times. Conversely, if the operation strategy requires low load cycling time and high RCCD, partial loading can limit the increase in the degradation rate. However, from an economic perspective, this is only feasible if the cost savings associated with the reduced degradation rate compensate for the increase in capital expenditure resulting from the lower capacity factor.

In the following example, the LCOH calculation model developed in [12], hourly electricity prices in Finland in 2024, and high and low capital costs assumptions of 2350 €/kWp and 550 €/kWp were used to compare between (a) the LCOH under dynamic load operation with constant increase in degradation rate (compared to steady-state operation), and (b) LCOH when degradation rate is dependent on the dynamic load operation parameters [12,46]. The degradation rate in steady-state operation mode was assumed to be 6 μV/h [37]. In the first scenario, the degradation rate at dynamic load operation was assumed to be 50% higher than the degradation rate at steady-state operation. In the second scenario, the LCOH was calculated at a load cycling time of 1 h and RCCD values of 0.003, 0.03, and 0.3 A/(cm^2·s). Fig. 11 shows the effect of degradation rate model and assumptions during dynamic load operation on LCOH at low and high capital cost boundaries.

In the first scenario, at high boundary, LCOH decreased from 7.37 €/kg in steady-state operation to 7.32 €/kg in dynamic load operation (0.67% decrease in LCOH). At low boundary, the LCOH decreased from 4.86 €/kg at steady-state operation to 3.8 €/kg at dynamic load operation (21.8% decrease in LCOH).

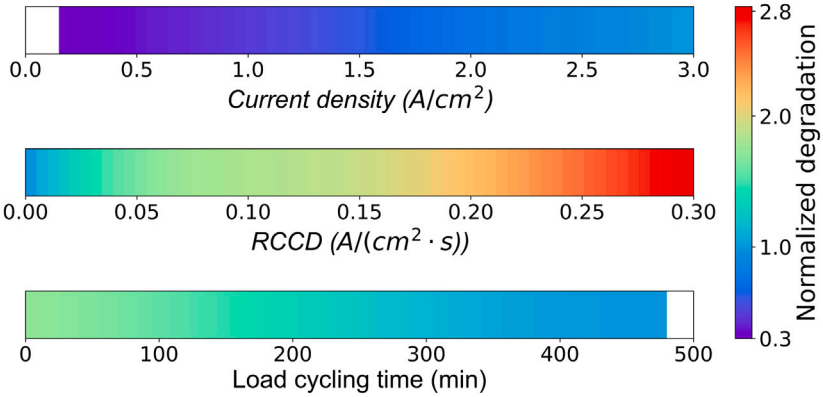

Fig. 9. Relation between dynamic load operation parameters and degradation rate of PEM stacks.

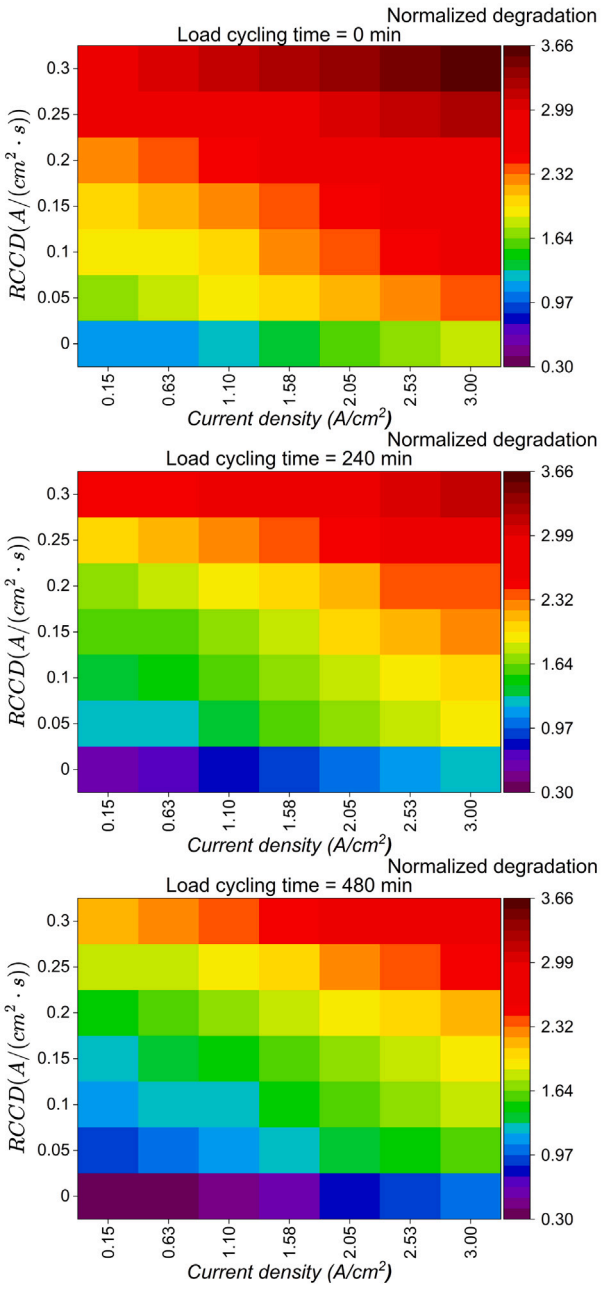

Fig. 10. Effect of dynamic load operation on the degradation rate of PEM stacks.

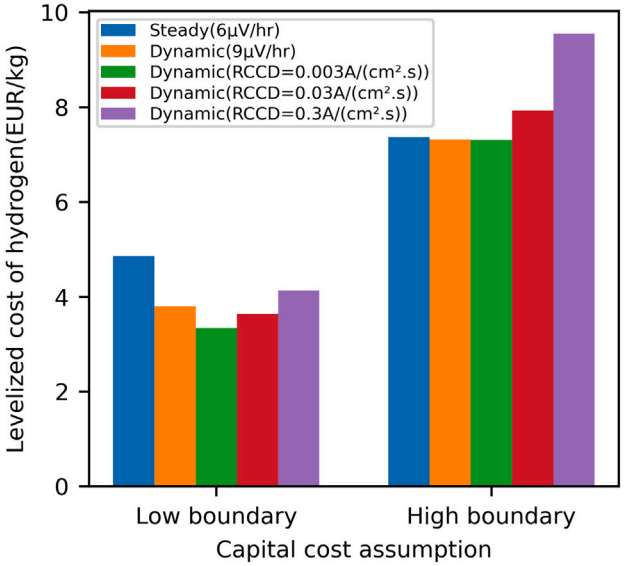

Fig. 11. Effect of degradation model on the levelized cost of hydrogen.

Conversely, in the second scenario, at high boundary, the LCOH at 0.003, 0.03, and 0.3 A/(cm^2·s) was 7.31 €/kg, 7.93 €/kg, and 9.55 €/kg, respectively. At high boundary and RCCD of 0.03 and 0.3 A/(cm^2·s), the LCOH in dynamic load operation was higher than the LCOH under steady-state operation by 7.6% and 29.6% respectively. Nevertheless, in the second scenario, at low boundary, the LCOH at 0.003, 0.03, and 0.3 A/(cm^2·s) was 3.34 €/kg, 3.64 €/kg, and 4.13 €/kg respectively. This corresponds to a decrease in LCOH, compared to steady-state operation, by 31.3%, 25.1%, and 15% respectively. Generally, accounting for the combined effect of dynamic load operation parameters on the degradation rate of PEM electrolyzer stacks increases the accuracy of techno-economic analysis and improves the optimization of PEM electrolysis operation.

4. Conclusions

Dynamic load operation of PEM electrolyzers results in a decreased LCOH, by exploiting lower electricity prices and participating in electricity reserve markets. However, these opportunities are dependent on the degradation rate of PEM electrolyzer stacks. As the ratio between the degradation rate in dynamic load operation and steady-state operation increases, green hydrogen cost rises due to the increase of the electrolyzer cost for replacement of stacks caused by degradation. Therefore, it is necessary to identify operational strategies to limit the increase in the degradation rate.

The degradation rate of PEM electrolyzer stacks can be characterized as a function of operating current density level, load cycling time, and RCCD. Partial loading of PEM electrolyzers prolongs the lifetime of the stacks. Therefore, operating the electrolyzer at rated current density, even in steady-state operation, may not represent the most effective approach. When conducting techno-economic analysis of electrolysis plants, different degradation rates at different operating current density levels should be considered in order to minimize the cost of green hydrogen. Moreover, in studies comparing degradation rates in steady-state and dynamic load operations, the average operating current density should be constant. This ensures that the study captures the effect of dynamic operation instead of the change in the current density.

The RCCD and load cycling time have a great impact on the degradation rate of PEM electrolyzer stacks. Minimizing the RCCD limits the increase in the degradation rate. This becomes vital when participating in electricity reserve markets. Different reserve markets have different technical requirements for response time. For example, frequency containment reserve for disturbances requires 86% of the reserve power to be activated in 7.5 s, while frequency containment reserve for normal operation requires 63% of the power to be activated in 1 min. Therefore, choosing the most suitable electricity reserve market, from technical and economic perspectives, is needed to decrease the LCOH.

Conversely, increasing the load cycling time decreases the degradation rate. Therefore, during dynamic load operation of PEM electrolyzers at high RCCD, a high load cycling time is preferable. However, if this is not possible due to technical or economic constraints, partial loading of PEM electrolyzers can be considered to limit the increase in the degradation rate.

In general, the degradation of PEM electrolyzer stacks can be predicted quickly and accurately by a DNN. With these features of the model, the optimization of electrolyzer operational strategies may be seamlessly embedded into the electricity market, taking into account its requirements regarding response times and operation parameters.

CRediT authorship contribution statement

H. Sayed-Ahmed: Writing – original draft, Visualization, Software, Methodology, Funding acquisition, Conceptualization. **R. Keller:** Writing – original draft, Investigation, Conceptualization. **Á.I. Toldy:** Writing – review & editing, Funding acquisition, Conceptualization. **M. Müller:** Writing – review & editing, Conceptualization. **D. Froning:** Writing – review & editing, Project administration, Conceptualization. **A. Santasalo-Aarnio:** Writing – review & editing, Supervision, Project administration, Funding acquisition, Conceptualization.

Declaration of competing interest

The authors declare the following financial interests/personal relationships which may be considered as potential competing interests: Hassan Sayed-Ahmed reports financial support was provided by Fortum and Neste Foundation. Hassan Sayed-Ahmed reports financial support was provided by Finland Fellowship. Hassan Sayed-Ahmed reports financial support was provided by The Finnish Foundation for Technology Promotion. If there are other authors, they declare that they have no known competing financial interests or personal relationships that could have appeared to influence the work reported in this paper.

Acknowledgments

The authors would like to thank Edward Rauls and Michael Hehemann for their extensive work on the test bench, which made the analyses presented here possible. H. Sayed-Ahmed would like to acknowledge funding from the Fortum and Neste Foundation, the Finnish Foundation for Technology Promotion, and The Finnish Ministry of Education and culture -Finland Fellowship.

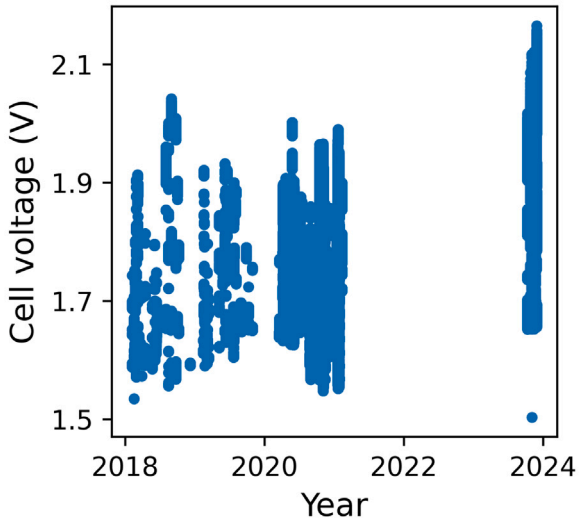

Fig. A.12. Experimental cell voltage as a function of date.

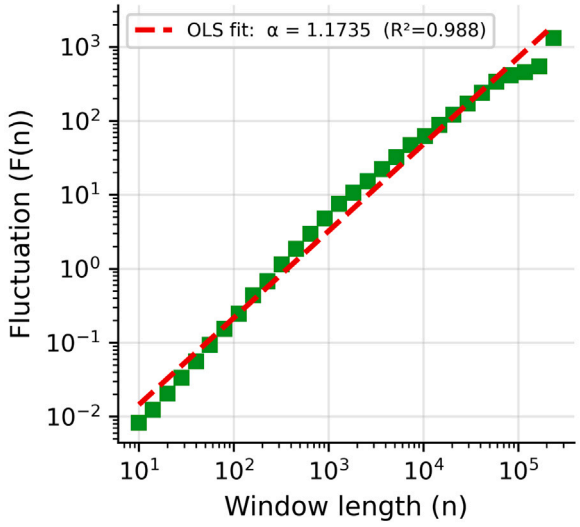

Fig. A.13. Log–log plot of detrended fluctuation analysis.

Appendix. Supplementary data

The experimental data represent 1134 h of operation measured over 6 years, totaling 945068 data points. Fig. A.12 shows the measured cell voltages of the two stacks as a function of date. The DNN model was built using a feed-forward architecture, which treats each data point independently, making it suitable to the large temporal gaps found within the experimental data.

Table A.3 states the minimum, maximum, and mean values of the input parameters used in the model.

To evaluate the long-range temporal dependencies in the dataset, detrended fluctuation analysis (DFA) was performed [47]. DFA was selected due to its robustness to non-stationarities arising from the intermittent nature of the dataset. Fig. A.13 illustrates the log–log relationship between window length and fluctuation function, whose slope, estimated via ordinary least squares regression, yields DFA scaling exponent ($\alpha = 1.17$). This value confirms that the dataset exhibits non-stationary dynamics with persistent long-range temporal correlations.

Fig. A.14 shows the code used to build the DNN model architecture.

```
import tensorflow as tf
normalizer = tf.keras.layers.Normalization(axis=-1)
normalizer.adapt(np.array(X_train_volt))
model = tf.keras.Sequential([normalizer,
                             tf.keras.layers.Dense(32, activation='mish'),
                             tf.keras.layers.Dense(32, activation='swish'),
                             tf.keras.layers.Dense(32, activation='mish'),
                             tf.keras.layers.Dense(32, activation='swish'),
                             tf.keras.layers.Dense(32, activation='linear'),
                             tf.keras.layers.Dense(32, activation='linear'),
                             tf.keras.layers.Dense(1)])

model.compile(optimizer=tf.keras.optimizers.Adam(learning_rate=0.0001),
              loss='MeanSquaredError',
              metrics=['RootMeanSquaredError','R2Score'])
callback = tf.keras.callbacks.EarlyStopping(patience=3)

history = model.fit(X_train_volt, y_train_volt, validation_split=0.2,
                    batch_size=16,epochs=100, verbose=1, callbacks=[callback])
loss_train = model.evaluate(X_train_volt,y_train_volt, batch_size=128, verbose=0)
loss_test = model.evaluate(X_test_volt,y_test_volt, batch_size=128, verbose=0)
```

Fig. A.14. Feed-forward deep neural network source code.

Table A.3
Input parameters range.

Parameters	Minimum	Median	Maximum	Unit
Load cycling time	0	32.1	498.9	minutes
Current density	0.15	0.95	2.34	A/cm^2
RCCD	0	0.00075	0.3	A/(cm^2·s)
Temperature	50	71.7	87.26	°C
Cathode pressure	2.02	4.88	5.5	bar
Anode pressure	1.025	3.98	4.3	bar
Flow rate in cathode	0.95	9.07	18.64	l/min
Flow rate in anode	4.14	7.74	16.37	l/min
Conductivity in cathode	0.00723	0.226	20	µS/cm
Conductivity in anode	0.132	0.622	2.69	µS/cm

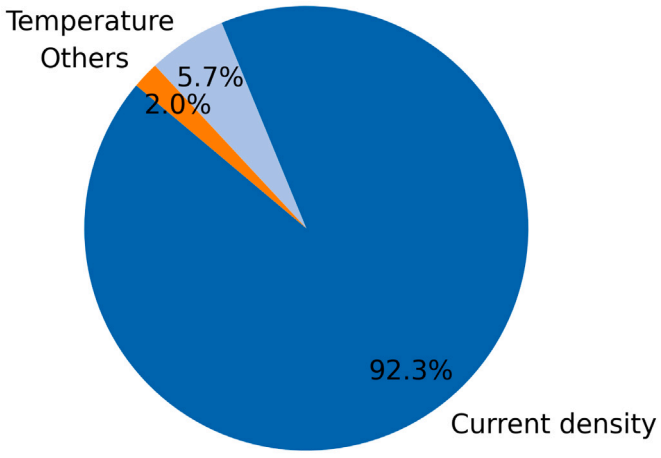

Fig. A.15. first-order Sobol sensitivity indices.

The Sobol method, using SALib python package, was applied to perform global sensitivity analysis on the trained DNN model [48,49]. Sobol method examines the influence of each input variable on the predicted voltage. Fig. A.15 shows the first-order Sobol sensitivity indices. Although 98% of the variance can be explained by the current density and temperature, the other parameters were still needed to keep the prediction error of the model within an acceptable range.

Data availability

Experimental data used in this study is openly available at https://doi.org/10.26165/JUELICH-DATA/FEKKSS, reference number [32].

References

[1] IEA. The future of hydrogen. Paris: International Energy Agency; 2019, Available from: https://www.iea.org/reports/the-future-of-hydrogen.

[2] Glenk G, Holler P, Reichelstein S. Advances in power-to-gas technologies: cost and conversion efficiency. Energy Environ Sci 2023;16(12):6058–70.

[3] Odenweller A, Ueckerdt F. The green hydrogen ambition and implementation gap. Nat Energy 2025;10(1):110–23.

[4] IRENA. Green hydrogen cost reduction: scaling up electrolysers to meet the 1.5° C climate goal. Abu Dhabi: International Renewable Energy Agency; 2020.

[5] Zun MT, McLellan BC. Cost projection of global green hydrogen production scenarios. Hydrogen 2023;4(4):932–60.

[6] Guerra OJ, Eichman J, Kurtz J, Hodge B-M. Cost competitiveness of electrolytic hydrogen. Joule 2019;3(10):2425–43.

[7] Lambert M, Barnes A, Marcu A, Imbault O, Bhashyam A, Tengler M, Cavallera C, Romeo G. 2024 State of the European hydrogen market report. The Oxford Institute for Energy Studies; 2024, Available from: https://www.oxfordenergy.org/publications/2024-state-of-the-european-hydrogen-market-report/.

[8] Hofrichter A, Rank D, Heberl M, Sterner M. Determination of the optimal power ratio between electrolysis and renewable energy to investigate the effects on the hydrogen production costs. Int J Hydrog Energy 2023;48(5):1651–63.

[9] Wang J, Wen J, Wang J, Yang B, Jiang L. Water electrolyzer operation scheduling for green hydrogen production: A review. Renew Sustain Energy Rev 2024;203:114779.

[10] Chung DH, Graham EJ, Paren BA, Schofield L, Shao-Horn Y, Mallapragada DS. Design space for PEM electrolysis for cost-effective H2 production using grid electricity. Ind Eng Chem Res 2024;63(16):7258–70. http://dx.doi.org/10.1021/acs.iecr.4c00123.

[11] Ginsberg MJ, Venkatraman M, Esposito DV, Fthenakis VM. Minimizing the cost of hydrogen production through dynamic polymer electrolyte membrane electrolyzer operation. Cell Rep Phys Sci 2022;3(6):100935, Available from: https://www.sciencedirect.com/science/article/pii/S2666386422002168.

[12] Sayed-Ahmed H, Toldy Á, Lappalainen M, Himanen O, Bajamundi C, Santasalo-Aarnio A. Strategies and challenges for reducing green hydrogen cost: Operation mode and revenue streams. Renew Sustain Energy Rev 2025;223:116065.

[13] Javed A, Wolf NL, Meyer F, Treutlein L, Kungl H, Karl A, Jodat E, Eichel R-A. Exploring the state-of-operation of proton exchange membrane electrolyzers. Int J Hydrog Energy 2025;98:280–94.

[14] Wallnöfer-Ogris E, Grimmer I, Ranz M, Höglinger M, Kartusch S, Rauh J, Macher-hammer M-G, Grabner B, Trattner A. A review on understanding and identifying degradation mechanisms in PEM water electrolysis cells: Insights for stack application, development, and research. Int J Hydrog Energy 2024;65:381–97.

[15] Maoulida F, Guilbert D, Camara M-B, Dakyo B. Dynamic electrical degradation of PEM electrolyzers under renewable energy intermittency: Mechanisms, diagnostics, and mitigation strategies – A comprehensive review. Renew Sustain Energy Rev 2026;225:116170.
[16] Lim D, Lee B, Lee H, Byun M, Cho H-S, Cho W, Kim C-H, Brigljević B, Lim H. Impact of voltage degradation in water electrolyzers on sustainability of synthetic natural gas production: Energy, economic, and environmental analysis. Energy Convers Manage 2021;245:114516.
[17] Campbell-Stanway C, Becerra V, Prabhu S. Techno-economic analysis with electrolyser degradation modelling in green hydrogen production scenarios. Int J Hydrog Energy 2025;106:80–95.
[18] Rakousky C, Reimer U, Wippermann K, Kuhri S, Carmo M, Lueke W, Stolten D. Polymer electrolyte membrane water electrolysis: Restraining degradation in the presence of fluctuating power. J Power Sources 2017;342:38–47, Available from: https://www.sciencedirect.com/science/article/pii/S0378775316316858.
[19] Papakonstantinou G, Algara-Siller G, Teschner D, Vidaković-Koch T, Schlögl R, Sundmacher K. Degradation study of a proton exchange membrane water electrolyzer under dynamic operation conditions. Appl Energy 2020;280:115911.
[20] Pantò F, Siracusano S, Briguglio N, Aricò AS. Durability of a recombination catalyst-based membrane-electrode assembly for electrolysis operation at high current density. Appl Energy 2020;279:115809.
[21] Sayed-Ahmed H, Toldy ÁI, Santasalo-Aarnio A. Dynamic operation of proton exchange membrane electrolyzers—Critical review. Renew Sustain Energy Rev 2024;189:113883, Available from: https://www.sciencedirect.com/science/article/pii/S1364032123007414.
[22] Gago AS, Bürkle J, Lettenmeier P, Morawietz T, Handl M, Hiesgen R, Burggraf F, Valles Beltran PA, Friedrich KA. Degradation of proton exchange membrane (PEM) electrolysis: The influence of current density. ECS Trans 2018;86(13):695–700.
[23] Frensch SH, Serre G, Fouda-Onana F, Jensen HC, Christensen ML, Araya SS, Kær SK. Impact of iron and hydrogen peroxide on membrane degradation for polymer electrolyte membrane water electrolysis: Computational and experimental investigation on fluoride emission. J Power Sources 2019;420:54–62, Available from: https://www.sciencedirect.com/science/article/pii/S0378775319302010.
[24] Feng Q, Yuan X-Z, Liu G, Wei B, Zhang Z, Li H, Wang H. A review of proton exchange membrane water electrolysis on degradation mechanisms and mitigation strategies. J Power Sources 2017;366:33–55.
[25] Chandesris M, Médeau V, Guillet N, Chelghoum S, Thoby D, Fouda-Onana F. Membrane degradation in PEM water electrolyzer: Numerical modeling and experimental evidence of the influence of temperature and current density. Int J Hydrog Energy 2015;40(3):1353–66, Available from: https://www.sciencedirect.com/science/article/pii/S0360319914032455.
[26] Alia SM, Stariha S, Borup RL. Electrolyzer durability at low catalyst loading and with dynamic operation. J Electrochem Soc 2019;166(15):F1164–72.
[27] Su Z, Liu J, Li P, Liang C. Study of the durability of membrane electrode assemblies in various accelerated stress tests for proton-exchange membrane water electrolysis. Materials 2024;17:1331.
[28] Voronova A, Kim S, Kim D, Park H, Jang J, Seo B. Systematic degradation analysis in renewable energy-powered proton exchange membrane water electrolysis. Energy Environ Sci 2023;16:5170.
[29] Pape S-V, Zerressen S, Seidler MF, Keller R, Lohmann-Richters F, Müller M, Apfel U-P, Mechler AK, Glüsen A. Performance data extraction from dynamic long-term operation of proton exchange membrane and alkaline water electrolysis cells. Int J Hydrog Energy 2025;127:51–63.
[30] He D, Chen K, Chen W, Luo Z, Xiong Z, Zou G, Li G, Chen B. Experimental study on the degradation of proton exchange membrane water electrolyzers under different dynamic loads and flow field configurations. J Power Sources 2025;641:236844.
[31] Xu B, Ma W, Wu W, Wang Y, Yang Y, Li J, Zhu X, Liao Q. Degradation prediction of PEM water electrolyzer under constant and start-stop loads based on CNN-LSTM. Energy AI 2024;18:100420.
[32] Keller R, Rauls E, Hehemann M, Müller M. Operational data of a 100 kw proton exchange membrane (PEM) electrolyzer: collection 2018–2023. Jülich DATA; 2025, http://dx.doi.org/10.26165/JUELICH-DATA/FEKKSS.
[33] Rauls E, Hehemann M, Scheepers F, Müller M, Peters R, Stolten D. System dynamics of polymer electrolyte membrane water electrolyzers and impact of renewable energy sources on systems design. Int J Hydrog Energy 2024;65:83–94, Available from: https://www.sciencedirect.com/science/article/pii/S0360319924011406.
[34] Rauls E, Hehemann M, Keller R, Scheepers F, Müller M, Stolten D. Favorable start-up behavior of polymer electrolyte membrane water electrolyzers. Appl Energy 2023;330:120350, Available from: https://www.sciencedirect.com/science/article/pii/S0306261922016075.
[35] Keller R, Rauls E, Hehemann M, Müller M, Carmo M. An adaptive model-based feedforward temperature control of a 100 kW PEM electrolyzer. Control Eng Pract 2022;120:104992, Available from: https://www.sciencedirect.com/science/article/pii/S096706612100263X.
[36] Keller R, Baader FJ, Bardow A, Müller M, Peters M. Experimental demonstration of dynamic demand response scheduling for PEM-electrolyzers. Appl Energy 2025;393:126014, Available from: https://www.sciencedirect.com/science/article/pii/S0306261925007445.
[37] Tsotridis G, Pilenga A. EU harmonised protocols for testing of low temperature water electrolysers. Luxembourg: Publications Office of the European Union; 2021.
[38] Misra D. Mish: A self regularized non-monotonic activation function. 2020, Available from: https://arxiv.org/abs/1908.08681.
[39] Ramachandran P, Zoph B, Le QV. Searching for activation functions. 2017, Available from: https://arxiv.org/abs/1710.05941.
[40] Weiß A, Siebel A, Bernt M, Shen T-H, Tileli V, Gasteiger H. Impact of intermittent operation on lifetime and performance of a PEM water electrolyzer. J Electrochem Soc 2019;166:F487–97.
[41] Lei J, G'Sell M, Rinaldo A, Tibshirani RJ, Wasserman L. Distribution-free predictive inference for regression. J Amer Statist Assoc 2018;113. http://dx.doi.org/10.1080/01621459.2017.1307116.
[42] Efron B, Tibshirani RJ. An introduction to the bootstrap. CHAPMAN & HALL/CRC; 1993.
[43] Bahr M, Gusak A, Stypka S, Oberschachtsiek B. Artificial neural networks for aging simulation of electrolysis stacks. Chem Ing Tech 2020;92(10):1610–7, Available from: https://onlinelibrary.wiley.com/doi/abs/10.1002/cite.202000089.
[44] Jung HY, Jun YS, Lee K-Y, Park HS, Cho SK, Jang JH. Effect of ramping rate on the durability of proton exchange membrane water electrolysis during dynamic operation using triangular voltage cycling. J Electrochem Sci Technol 2024;15(2):253–60.
[45] FINGRID. Reserve products and reserve market places. Helsinki: Fingrid Oyj; 2023, Available from: https://www.fingrid.fi/globalassets/dokumentit/en/electricity-market/reserves/reserve-products-and-reserve-market-places.pdf.
[46] ENTSO-E. European Network of Transmission System Operators for Electricity Transparency Platform. Available from: https://transparency.entsoe.eu/.
[47] Peng C-K, Buldyrev SV, Havlin S, Simons M, Stanley HE, Goldberger AL. Mosaic organization of DNA nucleotides. Phys Rev E 1994;49:1685–9, Available from: https://link.aps.org/doi/10.1103/PhysRevE.49.1685.
[48] Iwanaga T, Usher W, Herman J. Toward SALib 2.0: Advancing the accessibility and interpretability of global sensitivity analyses. Socio-Environmental Syst Model 2022;4:18155, Available from: https://sesmo.org/article/view/18155.
[49] Herman J, Usher W. SALib: An open-source python library for sensitivity analysis. J Open Source Softw 2017;2(9). http://dx.doi.org/10.21105/joss.00097.